Purpurin derivatives as visible-light photosensitizers for 3D printing and valuable biological applications

Purpurin derivatives as visible-light photosensitizers for 3D-printing and valuable biological applications

Pauline Sautrot-Ba,[1] *Vlasta Brezová,*[2] *Jean-Pierre Malval,*[3] *Annalisa Chiappone,*[4] *Samir Abbad-Andaloussi,*[5] *Davy-Louis Versace**[1]

[1]Université Paris-Est Créteil (UPEC), ICMPE–UMR-CNRS 7182, 2-8 rue Henri Dunant, 94320 Thiais, France.

[2]Slovak University of Technology in Bratislava, Institute of Physical Chemistry and Chemical Physics, Department of Physical Chemistry, Radlinského 9, SK-812 37 Bratislava, Slovak Republic.

[3]Institut de Chimie des Matériaux de Mulhouse (IS2M)-UMR 7361, 15 rue Jean Starcky - BP 2488, 68057 Mulhouse Cedex, France.

[4]Politechnico di Torino, Dipartimento di Scienza Applicata e Tecnologia, C. so Duca degli Abruzzi 24, 10129 Torino, Italy

[5]Université Paris-Est Créteil (UPEC), Laboratoire Eau, Environnement, Systèmes Urbains (LEESU), UMR-MA 102, 61 avenue Général de Gaulle, 94010 Créteil Cedex, France.

*Corresponding author: versace@icmpe.cnrs.fr

ABSTRACT. We report the synthesis of new visible-light photosensitizers derived from purpurin (mono-allyl- and triallyl- purpurin), and used as type II photoinitiating systems when associated with *N*-methyldiethanolamine, *bis*(4-methylphenyl) iodonium hexafluorophosphate or tri-functionalized thiol (trimethylolpropane *tris*(3-mercaptopropionate)), for the cationic and free-radical photopolymerization, and the initiation of thiol-ene reactions. These photoinitiating systems demonstrated good initiating properties in laminate or under air upon visible-light exposure *i.e.* LEDs@405 nm, 455 nm, 470 nm, 530 nm and Xe lamp. Steady-state photolysis, electron paramagnetic resonance, fluorescence and laser flash photolysis have clearly highlighted the photochemical properties of the different photoinitiating systems and proved that purpurin derivatives could act as electron donor or as proton/proton-coupled electron transfer promoter when associated with judicious additives. For the first time, we also demonstrated the capability of triallyl purpurin to produce new designed 3D-objects by 3D-photoprinting technology. Interestingly, the new 3D-materials incorporating triallyl- purpurin photosensitizer have undoubtedly pointed out tremendous antibacterial properties with a more than 99% of inhibition of bacterial adhesion upon visible-light exposure, even after many antibacterial cycle experiments, underlying thus their capability to be recycled.

Keywords. Purpurin; photopolymerization; 3D-printing; visible-light irradiation; antibacterial materials

INTRODUCTION

In the past decades, photo-driven reactions have attracted great interest in many chemistry domains, and become the cornerstone of a huge number of applications in microelectronics, adhesives, flooring, paving applications, photoresist technology, dentistry, and in the synthesis of novel biomaterials or 3D micro/nano objects[1, 2].

Photon-initiated chemical reactions become undoubtedly an indispensable process for the synthesis of original materials as it offers many striking advantages[3] over the thermal process including spatial control of the polymerization, low temperature conditions in solvent-free conditions, reduction of the reaction time, control of the overall properties of the photo-crosslinking materials, productivity increase and reduction of manufacturing costs using cheap, and new performing light sources[4] (*i.e.* light-emitting and laser diodes with visible or IR light emission). However, some main limitations can be pointed out such as oxygen-induced inhibition in free-radical photopolymerization[5] (FRP) or the use of harmful UV-light irradiation for the activation of petro-sourced photo-initiators[6]. The handling of safety issues and the high energy consumption associated with UV-light emitting sources have led to develop new performing visible-light photoactive systems[4, 7] to overcome previously described drawbacks. Both photocleavable Norrish type I and type II systems, acting in the visible or IR range, have been thus designed by molecular engineering[8]; their structures and photo-initiating properties have been extensively reviewed. However, the use of natural products as photoinitiator addressing both the environmental and safety concerns have somewhat been discarded up to now. The investigations on natural products as performing photo-initiators are scarce despite their potential for cutting off the synthesis costs of petro-sourced photo-initiators. Nevertheless, the first reports mentioning the use of riboflavin as free-radical photoinitiator of acrylic monomers[9, 10] were reported in the sixties, followed 40 years later, by some outstanding studies describing the photo-initiating properties of curcumin in the polymerizations of styrene[11], and

in the cationic photopolymerization (CP) of a variety of oxetane, epoxides, vinyl monomers[12] or epoxidized soybean oil[13]. In the same way, quercetin which is one of the most abundant flavones, was used for the first time as photosensitizer for the cationic photopolymerization of glycerol triglycidyl ether[14]. Recently, paprika, a carotenoid complex derivative was employed as a visible-light photosensitizer for the free-radical photoinduced cationic photopolymerization (FRPCP) of a gallic derived epoxy bio-based monomer[15]. Surprisingly, the largest class of naturally occurring quinones like purpurin and purpurin derivatives have been scarcely investigated as visible-light absorbing photosensitizers despite their high absorption properties in the visible range. Purpurin[16-18] is a crude madder extract and one of the main anthraquinone-type dyes discovered in the root, tubers of *Rubia tinctorum*, *R. peregrine*, *R. cordifolia*, and R. *munjista.* The limited studies describing the use of purpurin derivatives as visible-light photosensitizers for FRP or CP prompted us to design novel purpurin structures.

The originality of these new purpurin derived photosensitizers lies on their capability to be used as (i) visible-light absorbing photosensitizer for FRP and CP when wisely associated with co-initiators, (ii) they can be used to design 3D-objects by a 3D-photoprinting technique, in a reduced time, (iii) these derivatives could be covalently attached to the polymer network due to the presence of allyl photopolymerizable functionality and can be used as (iv) photoactive antimicrobial agent since they produce reactive oxygen species (ROS) under visible-light activation.

In this study, two purpurin derivatives (monoallylated purpurin (**PmA**) and triallylated purpurin (**PA**)) are synthesized and their photochemical behavior in comparison with the native purpurin (**P**) is evaluated under LEDs@385, 405, 455, 470 and 530 nm irradiation. The photoinitiating performance of both purpurin derivatives as photosensitizers for FRP or CP and thiol-ene process are investigated by real-time FTIR-spectroscopy and compared with the native purpurin. Photochemical mechanism details will be evidenced by steady-state photolysis,

nanosecond laser flash spectroscopy, fluorescence and electron paramagnetic resonance (EPR) experiments. In addition, and for the first time, the design of new 3D-objects by 3D-photoprinting technology from the tri-allylated purpurin (**PA**) derivative will be demonstrated. This is of great importance for the design of further complex medical devices. Finally, a new photoactive antimicrobial material derived from **PA** was tested against the adhesion of *Staphylococcus aureus* (*S. aureus*) under visible-light exposure after three antibacterial cycle experiments. The idea is to prove the reusability/recycling of our material and its antimicrobial performance against the adhesion of *S. aureus*, even after many antimicrobial tests.

EXPERIMENTAL

Materials. Purpurin (1, 2, 4-trihydroxyanthraquinone, **P**), 3,4-epoxycyclohexylmethyl 3,4-epoxycyclohexylcarboxylate (EPOX), trimethylolpropane *tris*(3-mercaptopropionate) (Trithiol, TT, >95%), *bis*(4-methylphenyl) iodonium hexafluorophosphate (Iod), 3-chloroperbenzoic acid (*m*-CPBA), tetrabutylammonium bromide (TBAB), 2,3,5,6-tetramethyl-1-nitrosobenzene (nitrosodurene, ND), *N*-*tert*-butyl-α-phenylnitrone (PBN) and 5,5-dimethyl-pyrroline *N*-oxide (DMPO, distilled prior to the application) were purchased from Sigma-Aldrich, and trimethylolpropane triacrylate (TMPTA) from Sartomer. *N*-methyldiethanolamine (> 98%) and allyl bromide (99%, stab. with 300-1000 ppm propylene oxide) were given by Alfa Aesar. Molecular sieves (3Å), silica gel, ethyl acetate (EtOAc), cyclohexane (CyH), diethyl ether (Et_2O) were obtained from Aldrich.

Synthesis of allyl purpurin derivatives (PmA and PA). Allyl purpurin derivatives were synthesized by microwave irradiation under non conventional phase transfer catalysis conditions[19]. Purpurin (**P**) (190 mg, 0.7 mmol, 1 equiv) was incorporated to a powder blend of NaOH (90 mg, 2.5 mmol, 3 equiv), K_2CO_3 (1.25 g, 9 mmol, 12 equiv) and TBAB (75 mg, 0.23 mmol, 0.3 equiv). Into a microwave tube (20 mL) containing allyl bromide (6 mL, 46 equiv),

resulting mixture was progressively added under agitation. Reaction was then carried out at 85 °C for 1 hour after which the sample was left to cool. The reacting solution was transfered into a separating funnel with 100 mL of deionized water and was extracted by Et_2O (3 x 50 mL). Organic phase was successively washed twice, dried under $MgSO_4$ and concentrated by vacuum evaporation. The final mixture was purified by silica gel chromatography (SiO_2, CyH/EtOAc 80/20) and two fractions were collected. The first fraction corresponds to the monoallylic derivative **PmA** (10 % yield, red powder), whereas the other fraction, a red oil (40 % yield), was refered to the triallylic purpurin **PA**.

^{1}H NMR of PA (400 MHz, $CDCl_3$, ppm, **Figure S1**): δ 8.18 – 8.13 (m, 1H, H2 or H13), 8.13 – 8.08 (m, 1H, H2 or H13), 7.70 – 7.61 (m, 2H, H1 and H14), 6.78 (s, 1H, H8), 6.23 (m, J = 16.5, 11.0, 6.0 Hz, 1H, H19), 6.07 (m, J = 16.1, 10.4, 5.0 Hz, 2H, H16 and H22), 5.61 (d, J = 16.5 Hz, 1H, H20b), 5.43 (t, J = 16.1 Hz, 2H, H17b and H23b), 5.34 (dd, J = 10.4, 2H, H17a and H23a), 5.25 (d, J = 11.0 Hz, 1H, H20a), 4.67 (dd, J = 5.0 Hz, 4H, H15 and H21), 4.58 (d, J = 6.0 Hz, 2H, H18). **^{13}C NMR of PA** (100 MHz, $CDCl_3$, ppm, Figures S2 and S3): δ 183.56 (C4 or C11), 181.53 (C4 or C11), 158.53 (C6 or C9), 157.33 (C6 or C9), 142.90 (C7), 134.67 (C5 or C10), 134.22 (C19), 134.16 (C5 or C10), 133.50 (C1 or C14), 132.88 (C1 or C14), 132.50 (C16 or C22), 131.93 (C16 or C22), 128.80 (C3 or C12), 126.56 (C2 or C13), 126.36 (C2 or C13), 118.52 (C17, C20 or C23), 118.27 (C17, C20 or C23), 118.13 (C17, C20 or C23), 115.56 (C3 or C12), 105.21 (C8), 74.83 (C18), 70.74 (C15 or C21), 69.80 (C15 or C21).

^{1}H NMR of PmA (400 MHz, $CDCl_3$, ppm, Figure S4): δ 13.54 (s, 1H, H15 or H19), 13.48 (s, 1H, H15 or H19), 8.36 (m, 2H, H2 and H13), 7.83 (m, 2H, H1 and H14), 6.71 (s, 1H, H8), 6.11 (m, J = 17.2, 10.4, 5.4 Hz, 1H, H17), 5.51 (d, J = 17.2 Hz, 1H, H18a), 5.41 (d, J = 10.4 Hz, 1H, H18b), 4.74 (d, J = 5.4 Hz, 2H, H16). **^{13}C NMR of PmA** (100 MHz, $CDCl_3$, ppm, Figures S5, S6): δ 187.41 (C4 or C11), 184.67 (C4 or C11), 160.80 (C6 or C9), 156.68 (C6 or C9), 150.60 (C7), 134.74 (C1 or C14), 134.19 (C5 or C10), 134.01 (C1 or C14), 133.41 (C5 or C10), 131.29

(C17), 127.15 (C2 or C13), 127.00 (C2 or C13), 119.79 (C18), 112.70 (C3 or C12), 108.14 (C8), 106.39 (C3 or C12), 70.39 (C16).

Characterization. ^{1}H and ^{13}C NMR spectra were recorded on a Bruker Avance II instrument at 400 MHz and 100 MHz, respectively. 1D and 2D NMR experiments were performed in $CDCl_3$. The UV-vis spectra were obtained on a Perkin Elmer Lambda 2 UV–vis spectrophotometer in the 200–800 nm wavelength range at room temperature.

Steady-state photolysis. Steady state photolysis experiments were performed under air with a LED@405 nm (M405L3-C4- Thorlab, 44 mW/ cm^2) in ACN. The photolysis of the purpurin derivatives were studied in the absence and in the presence of additives (Iod, MDEA, TT). Qualitative measurements of photoacids production were achieved by the addition of rhodamine B (RhB) as previously described[20].

Irradiation sources. Photopolymerizations were carried out with a conventional polychromatic Xenon lamp (Hamamatsu, Lightningcure LC8-03, xenon lamp, 200 W, 60 mW/ cm^2) and light-emitting diodes (LEDs) from Thorlabs (Newton, NJ, USA) with different emission wavelengths: LED@385 nm (44 mW/cm^2), LED@405 nm (60 mW/cm^2), LED@455 nm (38 mW/cm^2), LED@470 nm (25 mW/cm^2) and LED@530 nm (14 mW/cm^2).

Photopolymerization kinetic studies. Kinetic profiles of photocurable formulations were investigated by real-time Fourier transform infrared spectroscopy (RT-FTIR, Jasco FT-IR 4700). To monitor the progress of the reactions, the photosensitive formulations were spread on a BaF_2 pellet and irradiated under air or in laminate conditions with the above-mentioned LED sources. Acrylate or epoxy conversions were calculated by RT-FTIR by following the decrease of the acrylate or epoxy absorbance at 1640 and 790 cm^{-1}, respectively. The thickness of the photosensitive layer was estimated at 25 μm for all samples.

Cyclic Voltammetry. The cyclic voltammograms of the purpurin derivatives were recorded with an AUTOLAB potentiometer/ galvanometer employing GPES electrochemical software

version 4.9 (Utrecht, The Netherland). Substrates were introduced in a conventional three-electrode cell containing $NBuBF_4$ solution (acetonitrile, 0.1 mM) at 1 mM concentration. After performing an argon purge step, electrochemical measurements were carried out with a glassy carbon working electrode, a saturated calomel electrode (SCE) and a gold wire as a counter electrode as previously described[19, 20].

Laser flash photolysis (LFP). Laser flash photolysis study was achieved thanks to a Spectra Physics GCR-150-30 Nd:YAG laser at 355 nm with 7 ns impulsion time and a computer-controlled system which has been previously described in detail[20]. Analysis were conducted in a quartz cell (thickness = 1 cm) containing purpurin derivatives solution ([**P**] = 3.7 x 10^{-4} M, [**PmA**] = 3.8 × 10^{-4} M and [**PA**] = 2.1 × 10^{-4} M) which are degassed under argon during 10 min prior to LFP experiments.

Fluorescence studies. Fluorescence measurements were performed with a Perkin-Elmer Lambda 2 spectrometer and spectra were collected from a FluoroMax-4 spectrofluorometer.

EPR experiments. The EPR spectra in X-band (modulation frequency of 100 kHz) were measured by means of EMX*plus* spectrometer (Bruker) with the High Sensitivity Probe-head (Bruker) using the thin-walled quartz EPR tubes. The solutions prepared in benzene carefully saturated with argon were irradiated at 293 K directly in the EPR resonator using a LED@400 nm source (λ_{max} = 400 nm ; Bluepoint LED, Hönle UV Technology) or a LED@450 nm radiation (KL1600LED, Schott, blue filter), and the EPR spectra were recorded *in situ* during/after a defined exposure as described previously in [20]. The experimental EPR spectra were analyzed by WinEPR software (Bruker) and the calculations of simulated spectra were performed with the EasySpin toolbox working on MatLab® platform[21]. The detailed information on the EPR spectrometer settings are noted in the figure captions

Film preparation for antibacterial tests. The formulation containing EPOX/HEA (50%/50% w/w) in the presence of **PA**/Iod (0.5%/2.5% w/w) was poured into a silicon mould (1.5 cm x 2.5 cm x 0.3 cm) and was irradiated for 4 min under air with the LED@405 nm.

Singlet oxygen formation. The generation of singlet oxygen species was demonstrated by visible-light irradiation of PA in solution. The yield of the generated singlet oxygen was calculated in comparison with this generated by Rose Bengal (RB)[13]. RB was used as a standard photosensitizer ($\Phi_{\text{singlet oxygen (RB)}} = 0.68$ in ethanol)

Antibacterial Assays. The antibacterial properties of the the purpurin derived films under visible-light irradiation was evaluated against *S. aureus* ATCC6538. Experiments were done according to a previously described procedure[13-15]. The aim of the experiment is to evaluate the reusability of the films as antimicrobial materials.

3D-printing experiments. The 3D photosensitive formulation containing TT (20 wt%) / TMPTA (80 wt%) / **PA** (0.5 w%) was printed using a Asiga PICO 2 DLP printer with nominal XY resolution of 39 µm, using a diode as light-emitting source (405 nm; intensity 35 $mW.cm^{-2}$). Printing parameters were experimentally set as follows: a) layer thickness of 60 µm and b) layer exposure time of 2.4 s. A post curing process was performed during 5 min with a medium-pressure mercury lamp (12 $mW.cm^{-2}$, Robot Factory).

Results and discussion

The overall synthetic procedure for the synthesis of **PmA** and **PA** is shown in Scheme 1. NMR characterizations of the resulting purpurin derivatives are described in Supporting Information (Figures S1-S7). Actually, the synthesis of purpurin derivatives was done according to Williamson reaction[22]. This synthesis occured under microwave irradiation, using allyl bromide, in the presence of nucleophilic bases. After 1h reaction at 85 °C, the crude product was purified by flash chromatography on silica gel; 40% of the purified product corresponds to

the allylated purpurin (**PA**), and 10% is attributed to the monoallylated purpurin (**PmA**). ^{1}H NMR spectra of **PmA** and **PA** confirmed the success of the reactions with the presence of one and three allyl groups per purpurin moiety, respectively. The ^{1}H signals between 4.5 and 6.2 ppm are assigned to the protons of the allyl groups[19] of **PmA** and **PA**.

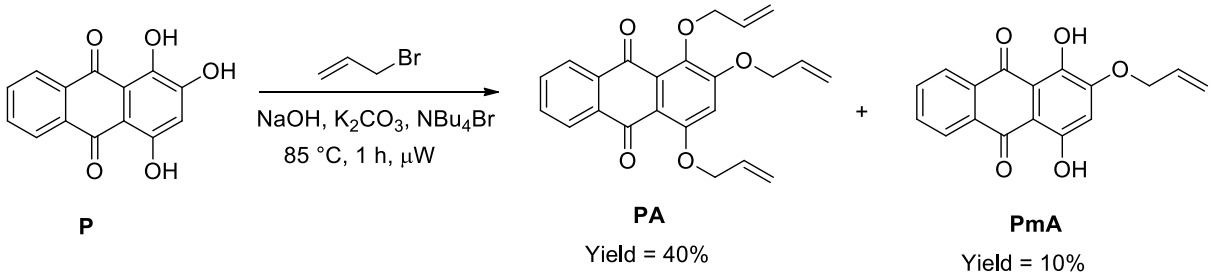

Scheme 1. Procedure for the synthesis of **PmA** and **PA**.

Light absorption properties of P, PmA and PA. The UV-vis absorption spectrum of **PA** shows an intense absorption bands located in the UV-visible range from 350 to 550 nm and centered at *ca* 400 nm (Figure S8). Contrary to **P** or **PmA** the addition of allyl groups on purpurin structure lead to a hypsochromic shift. Interestingly, the UV-vis absorption spectra of **PA** (λ_{max} = 401 nm, ε_{max} ~ 9600 M^{-1} cm^{-1}) and **PmA** (λ_{max} = 480 nm, ε_{max} ~ 6950 M^{-1} cm^{-1}) present a higher molar absorption coefficient than purpurin (**P**, λ_{max} = 477 nm, ε_{max} = 5974 M^{-1} cm^{-1}) or camphorquinone (CQ, λ_{max} = 466 nm, ε_{max} = 38 M^{-1} cm^{-1}), a well-established type II visible-light absorbing photoinitiator used in FRP and CP. The overlaps between the UV-vis absorption spectra of **PA** or **PmA** and the emission spectra of the LEDs@405, 455, 470 and 530 nm, make them very interesting as novel visible-light photosensitizers. Therefore, our attention is now focusing on the reactivity of the new purpurin derivatives in combination with different additives *i.e.* MDEA, Iod and TT. Their photochemical reactivity has been studied by EPR spin-trapping upon LED irradiation, by fluorescence and Laser Flash photolysis experiments. All the photochemical properties of the purpurin derivatives in combination with the co-initiators (Iod, MDEA or TT) are summarized in Table S1.

Photoreactivity of P, PmA and PA/Iod photoiniating systems. No EPR signals were found upon continuous *in situ* LED@450 nm photoexcitation of **P**/Iod/benzene solutions under argon, reflecting the limited lifetime of the photogenerated species. Consequently, the EPR spin trapping technique was applied to monitor the generation of (4-methyl)phenyl radical, using various spin trapping agents, *i.e.*, DMPO - a cyclic nitrone, PBN as the most reactive open-chain nitrone, and ND - a nitroso spin trap allowing the more detailed structure assignment of the trapped carbon-centered radical[23].

Experimental EPR spectra measured upon LED@450 nm irradiation of **P**/Iod/DMPO or **P**/Iod/PBN in benzene under argon along with their simulations were illustrated in Figure S9. The simulation analysis evidenced the trapping of (4-methyl)phenyl radical and formation of six-line signals of •DMPO-phenyl(4-methyl) or •PBN-phenyl(4-methyl) spin-adducts as the dominant spectral components. The spin-Hamiltonian parameters of (4-methyl)phenyl radical DMPO and PBN spin-adducts elucidated from the simulations of experimental EPR spectra are gathered in Table 1. The analogous EPR spectra of (4-methyl)phenyl radical spin-adducts were found upon LED@450 nm exposure of **PmA**/Iod/DMPO, **PmA**/Iod/PBN and **PmA**/Iod/ND (Figures S10 and S11), as well as LED@400 nm irradiation of **PA**/Iod/DMPO and **PA**/Iod/PBN (Figure 1) in benzene solutions under argon. Additionally, for both DMPO and PBN spin trapping agents, the signal of (4-methyl)phenyl adduct is superimposed with six-line signal of another carbon-centered-radical spin-adduct characterized by slightly altered spin-Hamiltonian parameters, *i.e.*, •DMPO-CR (a_N = 1.441±0.003 mT, a_H^β = 2.061±0.004 mT; g = 2.0061±0.0001) or •PBN-CR (a_N = 1.450±0.005 mT, a_H^β = 0.354±0.002 mT; g = 2.0061±0.0001), and the relative concentration of these spin-adducts increased upon the prolonged exposure. The photoexcitation of **PA**/Iod/ND (LED@400 nm) resulted in the exclusive generation of •ND-phenyl(4-methyl) spin-adduct and the monitored high-resolution experimental spectrum along with its simulation is shown in Figure S12.

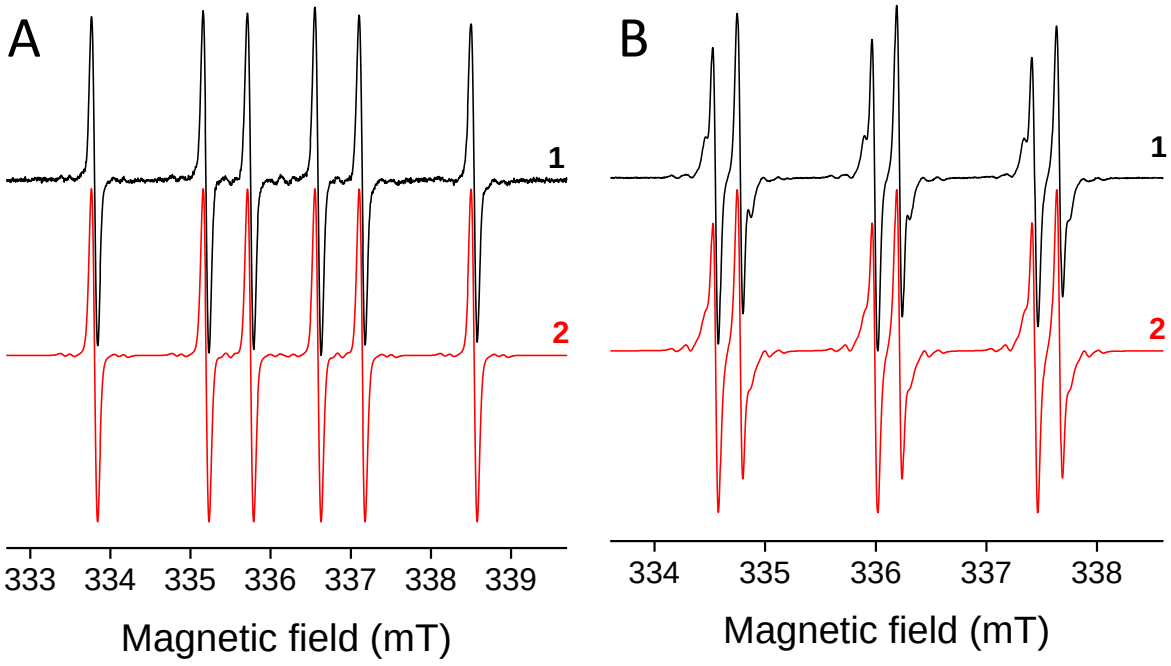

Figure 1. The normalized experimental (1) and simulated (2) EPR spectra obtained upon 900 s *in situ* LED@400 nm exposure of **PA**/Iod/benzene solution in the presence of spin trapping agent under argon. (**A**) DMPO; EPR spectrometer settings: microwave frequency, ~ 9.44 GHz; microwave power, 1.13 mW; center field, ~336.2 mT; sweep width, 7 mT; gain, 1.00×10^5; modulation amplitude, 0.025 mT; sweep time, 45 s; time constant, 10.24 ms; number of scans, 5. (**B**) PBN; EPR spectrometer settings: microwave frequency, ~ 9.44 GHz; microwave power, 1.12 mW; center field, ~336.2 mT; sweep width, 5 mT; gain, 2.00×10^4; modulation amplitude, 0.025 mT; sweep time, 45 s; time constant, 10.24 ms; number of scans, 5.

Table 1. The spin-Hamiltonian parameters of phenyl(4-methyl) spin-adduct elucidated from the simulations of the experimental EPR spectra measured upon irradiation of **P**, **PmA** or **PA** in the deoxygenated benzene solutions containing Iod and various spin trapping agents.

Spin trap	**a_N (mT)**	**a_H (mT)**	***g*-factor**

DMPO[a]	1.402±0.003	1.955±0.003	2.0060±0.0001
PBN[b]	1.452±0.003	0.221±0.0006	2.0061±0.0001
PBN (^{15}N)	2.106±0.003	0.293±0.003	2.0061±0.0001
ND	1.027±0.002	0.093±0.001, 0.093±0.001(H^{meta}) 0.287±0.002, 0.270±0.001 (H^{ortho}) 0.308±0.001, 0.308±0.001, 0.305±0.001 $(CH_3)^{para}$	2.0059±0.0001

[a] ^{13}C satellites 0.781 mT (2×^{13}C), 0.580 mT, 0.552 mT ; [b] ^{13}C satellites 0.749 mT (2×^{13}C), 0.492 mT (4×^{13}C)[24]

These statements are further confirmed indirectly under light irradiation by steady-state photolysis, fluorescence and LFP experiments. As described Figures S13-S15, the addition of Iod to purpurin derivatives leads to the decrease of their visible absorption band upon LED@405nm irradiation, demonstrating a synergistic interaction. Another interesting feature is the formation of Brønsted acids H^+ after the photolysis of purpurin derivatives/Iod systems according to a previously described test involving rhodamine B: indeed, H^+ are captured by rhodamine B, leading to the increase of the 550 nm absorbance of the acid form of rhodamine B[13]. The fluorescence properties of both **P**, **PmA** and **PA** and their quenching by Iod are displayed in Figure S16. **P**, **PmA** and **PA** show fluorescence at 575 nm, 575 nm and 560 nm, respectively. The fluorescence quenching constants K_{SV} of **P**, **PmA** and **PA** by Iod were evaluated at 40 M^{-1}, 3 M^{-1} and 9.5 M^{-1}, Figure S16) and highlight a possible electron transfer reaction between the singlet excited states of purpurin derivatives and Iod. The negative free energy changes of **P**, **PmA** and **PA** with Iod (i.e. $\Delta G_{S\,(\mathbf{P}/Iod)}$ = -0.61 eV , $\Delta G_{S\,(\mathbf{PmA}/Iod)}$ = -0.43 eV and $\Delta G_{S\,(\mathbf{PA}/Iod)}$ = -0.24 eV) calculated from the Rehm-Weller equation[25] using the oxidation potentials (E_{ox}(**P**) = 1.35V, E_{ox}(**PmA**) = 1.53V and E_{ox}(**PA**) = 1.77V measured by cyclic voltammetry; see Supporting Information, Figure S17), the reduction potential of Iod ($E_{Red,Iod}$ = -0.2 V) and the excited singlet state energies of the purpurin derivatives ($E_{S,\mathbf{P}}$ = 2.16 eV, $E_{S,\mathbf{PmA}}$ = 2.16 eV and $E_{S,\mathbf{PA}}$ = 2.21 eV extracted from the emission fluorescence spectra) are in

full agreement with an electron transfer reaction from ^{1}**P*** (^{1}**PmA*** or ^{1}**PA***) to Iod. Interestingly, the triplet excited lifetime of **P**, **PmA** and **PA** decreased after the addition of Iod. Several triplet state absorption peaks for **P**, **PmA** and **PA** have been clearly observed at 410, 500 or 560 nm (see Figure S18). The bimolecular rate constants for the quenching of ^{3}**P*,** ^{3}**PmA*** and ^{3}**PA*** by Iod (*i.e*. k_q^{Iod} (^{3}**P***), k_q^{Iod} (^{3}**PmA***) and k_q^{Iod} (^{3}**PA***)) have been calculated from the plot of the slope of the inverse triplet lifetime *vs* Iod concentration (see Supporting Information, Figure S19). Therefore, k_q^{Iod} (^{3}**PmA***) = 5±0.8 × 10^9 $M^{-1}s^{-1}$ (at 410 nm) and k_q^{Iod} (^{3}**PA***) = 1.1±0.2 × 10^8 $M^{-1}s^{-1}$ at 560 nm (Supporting Information, Figure S19), thus demonstrating an electron transfer reaction between ^{3}**PmA*** or ^{3}**PA***and the ground state of Iod, contrary to ^{3}**P*** and Iod which triplet state quenching was not observed. Interestingly, a new LFP signal could be observed at 700 nm (with a lifetime > 150 μs) after the **PA**/Iod photolysis (Figure S20). As previously described by Pappas et al.[26], this later signal can be attributed to the 4-methylphenyliodinium radical cation ($MePhI^{\bullet+}$). The overall mechanism involving purpurin derivatives and Iod are described in Scheme 2. These statements have been previously described and confirmed indirectly by LFP, EPR spin-trapping and steady-state photolysis experiments. For more clarity, we only present the mechanism involving **PA** which can occur at the singlet or triplet excited state. The oxidation of **PA** singlet or triplet excited state by Iod leads to the decomposition of the unstable $(MePh)_2I^{\bullet}$ to iodomethylbenzene and 4-methylphenyl radical ((steps 2 and 6), according to EPR experiments). The formation of $MePhI^{\bullet+}$ (step 3) is confirmed by LFP and further step reactions photoacids (H^+) are generated (see steady-state photolysis of purpurin derivatives, Figures S13C, S14C and S15C). The formation of H^+ is also indirectly confirmed by cationic photopolymerization of epoxy monomers (see kinetic studies).

PA $h\nu \rightarrow {}^{1,3}$**PA*** (1)

^{1,3}**PA*** **+** $(MePh)_2I^+$ (Iod) → $\mathbf{PA}^{\bullet+}$ + $(MePh)_2I^{\bullet}$→ $\mathbf{PA}^{\bullet+}$ + $MePh^{\bullet}$ + MePhI (2)

MePhI + **PA** → $MePhI^{\bullet+}$ + $\mathbf{PA}^{\bullet-}$ (3)

$MePhI^{\bullet+}$ + MePhI → $[MePhI\text{-}PhMeI]^{\bullet+}$ (4)

$[MePhI\text{-}PhMeI]^{\bullet+}$ + $(MePh)_2I^+$ → $[MePhI^+\text{-}PhMeI]$ + H^+ + $(MePh)_2I^{\bullet}$ (5)

$(MePh)_2I^{\bullet}$ → $MePh^{\bullet}$ + MePhI (6)

Scheme 2. Photoinduced generation of radical species from the photolysis of **PA**/Iod.

Photoreactivity of P, **PmA and PA/MDEA photoiniating systems.** In the presence of amines, the photoexcited hydroxyanthraquinones (HAQ) behave as the efficient electron acceptor[27, 28] generating the corresponding anthrasemiquinones (radical anions) detectable by cw-EPR spectroscopy[29-31]. Consequently, the EPR signal (g = 2.0043) with the unresolved hyperfine structure (Figure S21) measured upon LED@450 nm irradiation of **P**/MDEA solution in benzene under argon was assigned to the purpurin anthrasemiquinone[32]. This paramagnetic species is detectable also in the irradiated solution **P**/MDEA/DMPO/benzene/Ar, especially upon the prolonged LED@450 nm exposure, and simultaneously two DMPO-adducts are produced reflecting the trapping of reactive radical species formed *via* $MDEA^{\bullet+}$ transformation, *i.e.*, aminoalkyl radical DMPO-adduct[33] (a_N = 1.461±0.001 mT, a_H^{β} = 1.788±0.008 mT, a_H^{γ} = 0.115±0.001 mT, a_H^{γ} = 0.074±0.002 mT; g = 2.0058±0.0001) and carbon-centered radical DMPO-adduct (a_N = 1.468±0.002 mT, a_H^{β} = 2.024±0.010 mT; g = 2.0059±0.0001) (Figure S22). The stability of DMPO-adducts is low, and after radiation cut-off they immediately disappeared from spectra. The irradiation of **PmA**/MDEA/DMPO/benzene/Ar (LED@450 nm, Figure S23A) or **PA**/MDEA/DMPO/benzene/Ar (LED@400 nm, Figure 2A) resulted in the generation of both DMPO-adducts, with the prevailing signal of DMPO-adduct with aminoalkyl radical. The EPR spectra of the corresponding anthrasemiquinones were measured in the DMPO-free systems, irradiating the deoxygenated benzene solutions of

PmA/MDEA (Figure S23B) or **PA**/MDEA (Figure 2B), and the slightly better resolved spectra allow to estimate the approximate hyperfine coupling constants of hydrogen nuclei (Table 2). Further experimental evidence for the purpurin derivatives'interaction with MDEA was given by steady-state photolysis, fluorescence and LFP experiments. The addition of MDEA leads, whatever the nature of purpurin derivatives, to a strong decrease of their absorbance between 400 and 500 nm (Figure S13D, S14D and S15D). The fluorescence quenching constants K_{SV} of **P** and **PmA** by MDEA were evaluated at 4800 M^{-1} and 13 M^{-1} (Figures S24A and S24B, respectively). No fluorescence quenching was observed between the singlet excited state of **PA** and MDEA. Interestingly, only the triplet excited lifetimes of **PmA** (Figure S25) and **PA** (Figure 3) decreased when MDEA is added. The bimolecular rate constants for the quenching of ^{3}**PmA*** and ^{3}**PA*** by MDEA (*i.e.* k_q^{MDEA} (^{3}**PmA***) and k_q^{MDEA} (^{3}**PA***)) were respectively evaluated at $2\pm0.1 \times 10^7$ $M^{-1}s^{-1}$ at 410 nm, and $7\pm0.6 \times 10^8$ $M^{-1}s^{-1}$ at 560 nm. The EPR and LFP experiments undoubtedly confirm an electron transfer reaction followed to a proton transfer process from MDEA to **PA** (eq 7).

$$\mathbf{PA} + \text{MDEA } h\nu \rightarrow \mathbf{PAH}^{\bullet} + \text{MDEA}^{\bullet}_{(-H)} \quad (7)$$

Table 2. The spin-Hamiltonian parameters of anthrasemiquinones estimated from the simulations of the experimental EPR spectra measured upon irradiation of **P**, **PmA** (LED@450 nm) or **PA** (LED@400 nm) in the deoxygenated benzene solutions containing MDEA.

HAQ	a_H **(mT)**	***g*-factor**
P	not resolved	2.0043±0.0001
PmA	0.130 (2H), 0.124 (1H), 0.074 (2H), 0.062 (2H)	2.0040±0.0001
PA	0.174 (1H), 0.114 (1H), 0.106 (2H), 0.066 (1H)	2.0041±0.0001

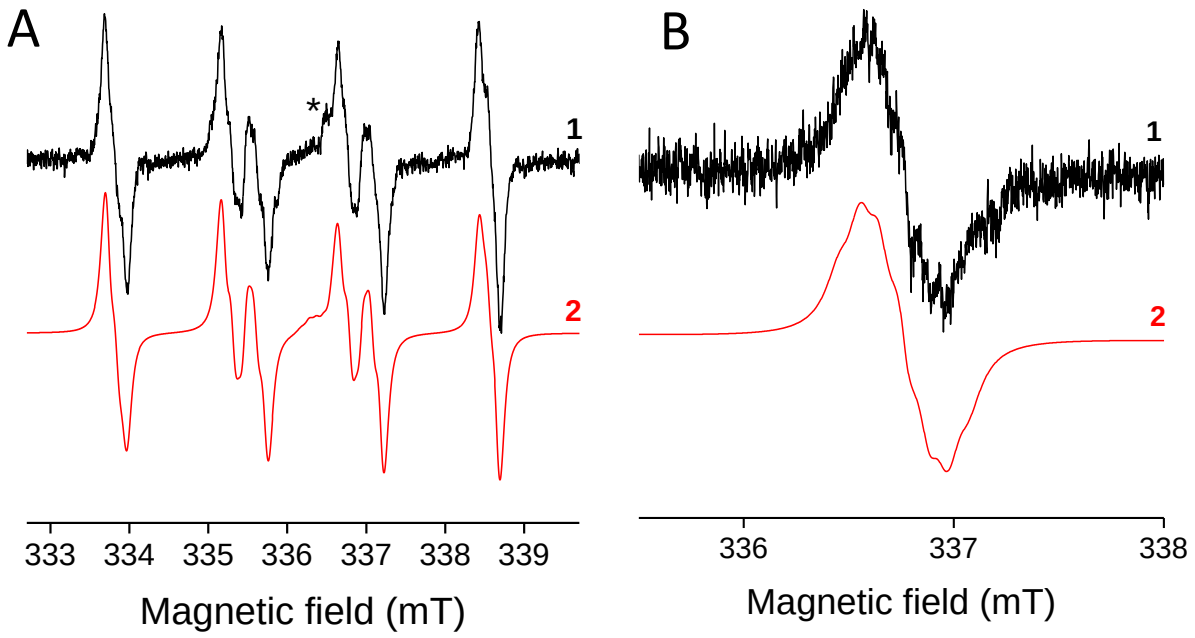

Figure 2. The normalized experimental (1) and simulated (2) EPR spectra obtained upon 900 s *in situ* LED@400 nm exposure of benzene solutions under argon. (**A**) **PA**/MDEA/DMPO (* denotes signal of **PA** anthrasemiquinone radical); EPR spectrometer settings: microwave frequency, ~ 9.44 GHz; microwave power, 11.22 mW; center field, ~336.2 mT; sweep width, 7 mT; gain, 1.00×10^5; modulation amplitude, 0.025 mT; sweep time, 45 s; time constant, 10.24 ms; number of scans, 5 and (**B**) **PA**/MDEA; EPR spectrometer settings: microwave frequency, ~ 9.45 GHz; microwave power, 1.16 mW; center field, ~336.8 mT; sweep width, 2 mT; gain, 1.00×10^5; modulation amplitude, 0.05 mT; sweep time, 45 s; time constant, 10.24 ms; number of scans, 10.

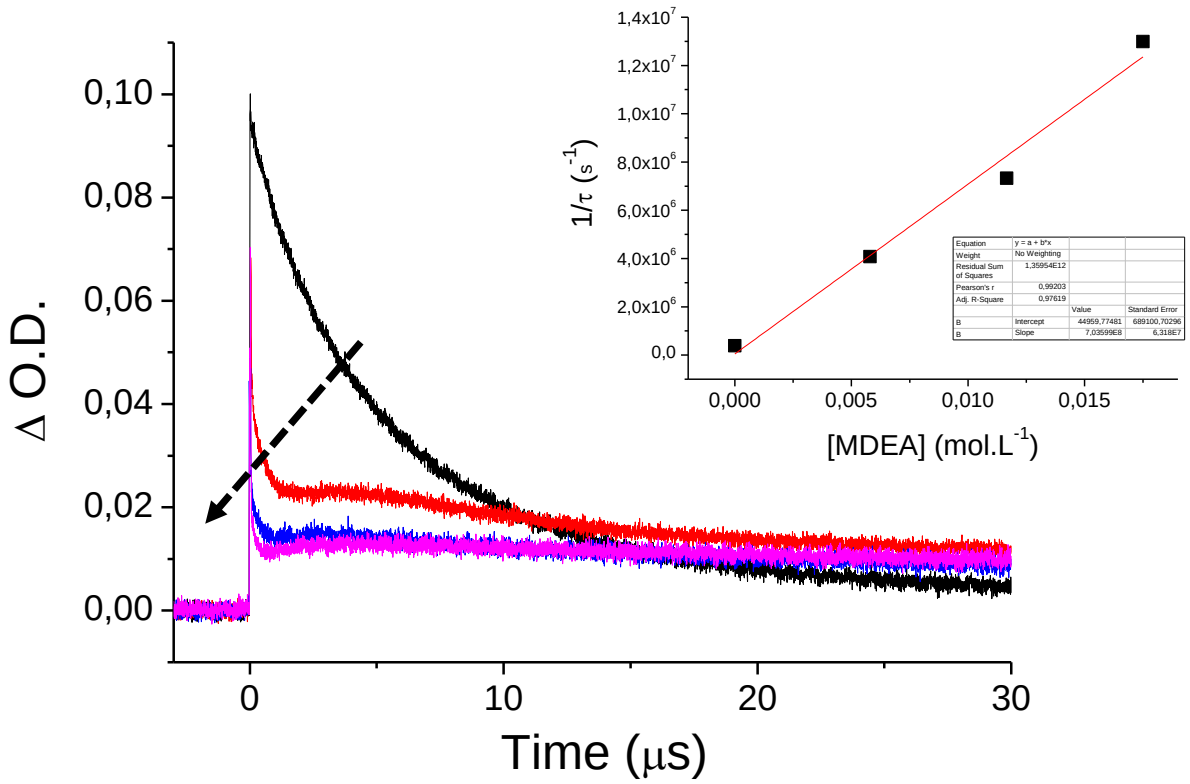

Figure 3. Decay traces of **PA**/MDEA at 560 nm in ACN under argon atmosphere (λ_{ex} = 355 nm). **Inset:** Determination of the bimolecular quenching rate constants k_q^{MDEA} (^{3}**PA***) using LFP (λ_{ex} = 355 nm, 7 ns pulse width). Pseudo-first-order decay rate constant of ^{3}**PA*** monitored at 560 nm *vs*. varying concentration of MDEA.

Photoreactivity of P, **PmA and PA/TT photoiniating systems.** Upon photoexcitation of **P**, **PmA** and **PA** in the deoxygenated benzene solutions containing TT and DMPO, the analogous EPR spectra were measured in all photoinitiating systems, and the spin-Hamiltonian parameters elucidated from the simulation spectra, *i.e.* a_N = 1.347±0.003 mT, a_H^{β} = 1.173±0.003 mT, a_H^{γ} = 0.090±0.004 mT, a_H^{γ} = 0.097±0.005 mT; g = 2.0061±0.0001) correlate well with the generation of DMPO-adduct with thiyl radical •DMPO-SR (Figures S26A, S27A, and Figure 4A for **P**/TT, **PmA**/TT and **PA**/TT respectively). The addition of Iod in these photoinitiating systems resulted in the simultaneous generation of two DMPO-adducts[20, 33], *i.e.*, •DMPO-phenyl(4-methyl) and •DMPO-SR, as is shown in Figures S26B (**P**/TT/Iod), S27B

(**PmA**/TT/Iod) and Figure 4B (**PA**/TT/Iod). The stability of DMPO-adducts is very low, after radiation cut-off they disappeared from spectra. Steady-state photolysis confirm a synergistic interaction between **P**, **PmA** and **PA** ground state and TT as their absorption band rapidly drops down after the addition of TT under light irradiation (Figures S13E, S14E and S15E). Suprisingly, only the singlet excited state of **PmA** is quenched by TT with a fluorescence quenching constant $K_{SV\ (PmA/TT)}$ = 1 M^{-1} (Figure S28). Interestingly, only the triplet excited lifetimes of **P** and **PA** decreased when TT is added. The bimolecular rate constants for the quenching of ^{3}**P*** and ^{3}**PA*** by TT (*i.e.* k_q^{TT} (^{3}**P***) and k_q^{TT} (^{3}**PA***)) were respectively evaluated at 2.4±0.2 × 10^7 $M^{-1}s^{-1}$ at 410 nm (Figure S29), and 1.2±0.1 × 10^8 $M^{-1}s^{-1}$ at 560 nm (Figure 5). The corresponding mechanism without Iod is described as follow (eq 8).

Purpurin derivative + RSH **(**h*ν*) → protonated purpurin derivative radical + $RS^{\bullet}$ (8)

When Iod is added to purpurin derivatives/TT system, a similar mechanism could be observed than that of (eq 8) but the formation of MePh radical in the medium should be taken into consideration as follow (eq 9). MePh radical can be involved in a H-abstraction reaction, generating thus thyil radicals.

$MePh^{\bullet}$ + RSH **(**h*ν*) → MePh-H + $RS^{\bullet}$ (9)

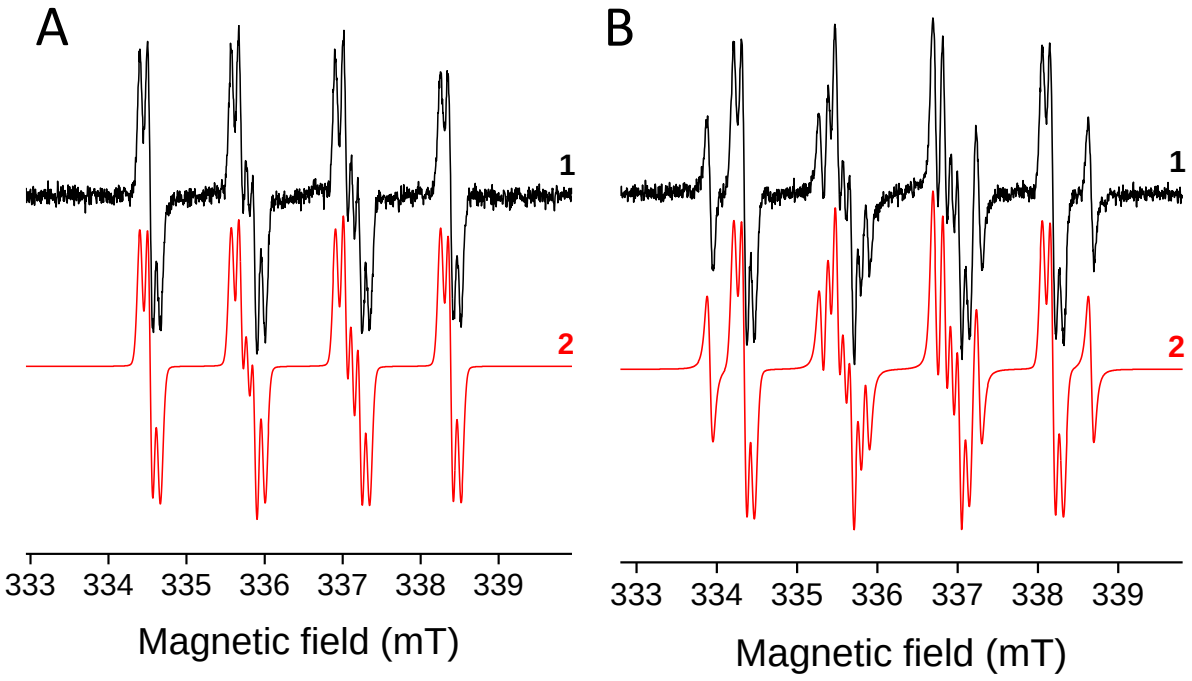

Figure 4. The normalized experimental (1) and simulated (2) EPR spectra obtained upon *in situ* LED@400 nm irradiation of benzene solutions under argon: (**A**) **PA**/TT/DMPO, exposure 225 s; EPR spectrometer settings: microwave frequency, ~ 9.45 GHz; microwave power, 1.16 mW; center field, ~336.4 mT; sweep width, 7 mT; gain, 1.00×10^5; modulation amplitude, 0.025 mT; sweep time, 45 s; time constant, 10.24 ms; number of scans, 5. (**B**) **PA**/TT/Iod/DMPO, exposure 450 s; EPR spectrometer settings: microwave frequency, ~ 9.44 GHz; microwave power, 1.13 mW; center field, ~336.3 mT; sweep width, 7 mT; gain, 1.00×10^5; modulation amplitude, 0.025 mT; sweep time, 45 s; time constant, 10.24 ms; number of scans, 10.

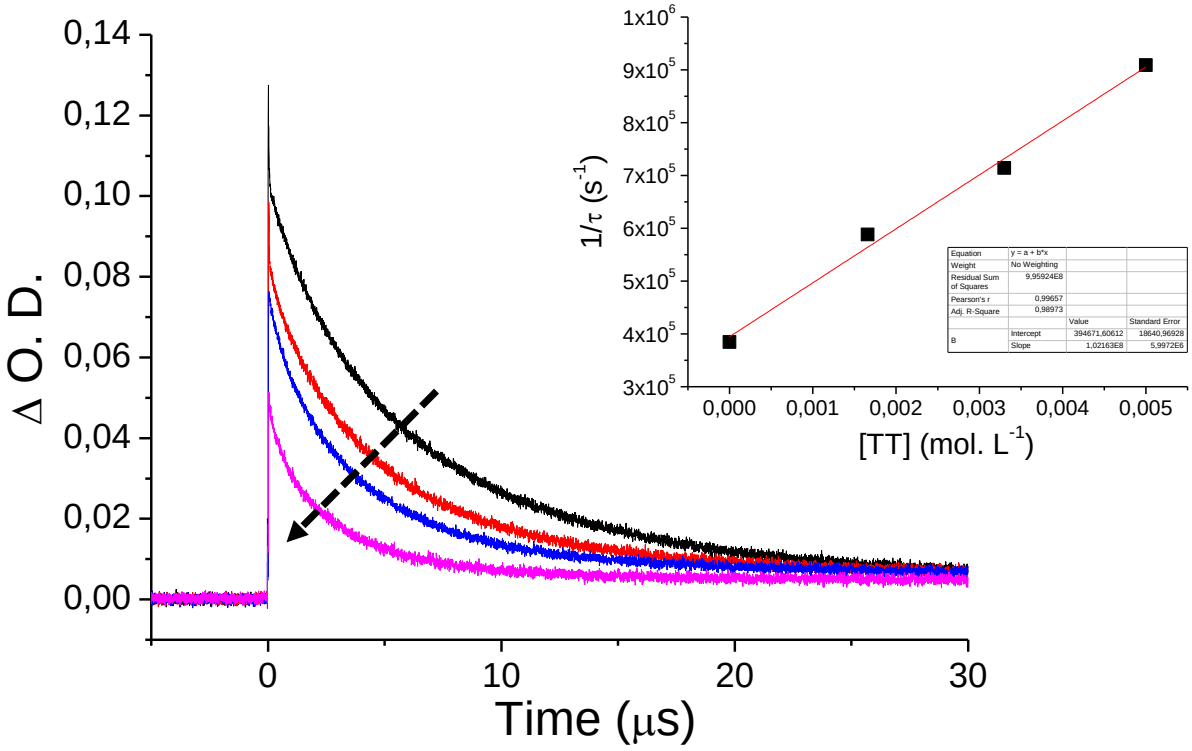

Figure 5. Decay traces of **PA**/TT at 560 nm in ACN under argon atmosphere (λ_{ex} = 355 nm). **Inset:** Determination of the bimolecular quenching rate constants k_q^{TT} (^{3}**PA***) using LFP (λ_{ex} = 355 nm, 7 ns pulse width). Pseudo-first-order decay rate constant of ^{3}**PA*** monitored at 560 nm *vs*. varying concentration of TT.

Kinetic studies. Different photoinitiating systems including the three purpurin derivatives have been described by RT-FTIR by following the epoxy and acrylate conversions of EPOX and TMPTA/HEA monomers respectively under different LEDs irradiation wavelengths (Table 3). The kinetic results on FRP are in agreement with EPR data and all are described in supporting information (Figures S30-S45): Indeed, the addition of co-initiator (Iod, MDEA or TT) to purpurin derivatives led respectively to 4-methylphenyl, aminoalkyl and thiyl radicals which can initiate FRP in laminate. Kinetic profiles and conversions are less efficient under air as oxygen is well-known to be a scavenger of radicals species[5], inhibiting thus the FRP. However, Table 3 underlines also the high reactivity of **PA** in comparison with **P** or **PmA** with regards to FRP and CP under air and in laminate. In light of LFP and fluorescence results, it seems that

photochemical pathways with **PA** occur mainly in its triplet excited state ; and surprisingly the bimolecular rate constants for the quenching of ^{3}**PA*** (2×10^8 $M^{-1}s^{-1}$ at 560 nm) by O_2 is quite lower than that of ^{3}**P*** (3.4×10^8 $M^{-1}s^{-1}$ at 410 nm) and ^{3}**PmA*** (3.7×10^8 $M^{-1}s^{-1}$ at 410 nm) with oxygen (Figure S46). This could explain the better reactivity of **PA** photoinitiating systems under air than those containing **P** or **PmA** towards acrylate monomers. The other reason which could be evoked for the lower reactivity of **P** or **PmA** *vs* **PA** is that phenolic purpurin can interact with the active radical species generated in the bulk during the photoinduced polymerization reaction; the generated phenoxyl radicals could act as efficient termination agents, inhibiting thus the growing polymer chains and the FRP[34]. Another interesting feature according to EPR data is the generation under light exposure of new carbon-radical species when **PA** is employed. The additional formation of these carbon-radical species may explain the increase of acrylate conversions in comparison with **P** and **PmA** derived photoinitiating systems. Interestingly, final epoxy or acrylate conversions with **PA** derived photoinitiating systems are higher than those described in literature specially with camphorquinone[19].

Table 3. Epoxy and acrylate conversions (%, determined by IR) of EPOX and TMPTA/HEA monomers respectively, upon LED@385, 405, 455, 470, 530 nm, and Xe lamp irradiation for 800s in laminate or under air, in the presence of the **P, PmA** and **PA** derived photoinitiating systems.

		Irradiation Wavelength (ƛ) (nm)					
Formulations	**Polymerization system**	**385**	**405**	**455**	**470**	**530**	**Xe lamp**
P/Iod/TMPTA	Acrylate	31[a], np[b]	40[a], np[b]	np[a], np[b]	np[a], np[b]	np[a], np[b]	np[a], np[b]
P/TT/TMPTA	Acrylate	90[a], np[b]	92[a], np[b]	42[a], np[b]	31[a], np[b]	np[a], np[b]	75[a], np[b]
	Thiol (TT)	43[a], np[b]	46[a], np[b]	30[a], np[b]	23[a], np[b]	np[a], np[b]	30[a], np[b]

P/Iod/TT/TMPTA	Acrylate	95[a], 74[b]	98[a], 95[b]	72[a], 46[b]	47[a], np[b]	18[a], np[b]	85[a], np[b]
	Thiol (TT)	48[a], 35[b]	50[a], 35[b]	30[a], 47[b]	28[a], np[b]	10[a], np[b]	34[a], np[b]
P/MDEA/TMPTA	Acrylate	37[a], np[b]	22[a], np[b]	10[a], np[b]	np[a], np[b]	np[a], np[b]	13[a], np[b]
P/Iod/EPOX	Epoxy	30[b]	20[b]	6[b]	np[b]	np[b]	np[b]
P/Iod/EPOX/TMPTA	Acrylate	70[a], np[b]	71[a], np[b]	np[a], np[b]	21[a], np[b]	np[a], np[b]	85[a], np[b]
	Epoxy	51[a], np[b]	50[a], np[b]	np[a], np[b]	17[a], np[b]	np[a], np[b]	36[a], np[b]
P/Iod/HEA	Acrylate	71[a], 37[b]	76[a], 62[b]	62[a], 16[b]	50[a], np[b]	23[a], np[b]	54[a], 21[b]
P/Iod/HEA/EPOX	Acrylate	85[a], 23[b]	91[a], 56[b]	55[a], np[b]	52[a], np[b]	20[a], np[b]	75[a], np[b]
PmA/Iod/TMPTA	Acrylate	41[a], np[b]	32[a], np[b]	12[a], np[b]	12[a], np[b]	np[a], np[b]	np[a], np[b]
PmA/ TT/TMPTA	Acrylate	88[a], 78[b]	94[a], 89[b]	85[a], 73[b]	80[a], np[b]	61[a], np[b]	85[a], np[b]
	Thiol (TT)	43[a], 32[b]	45[a], 49[b]	44[a], 35[b]	32[a], np[b]	27[a], np[b]	39[a], np[b]
PmA/Iod/TT/TMPTA	Acrylate	95[a], 99[b]	98[a], 99[b]	94[a], 87[b]	89[a], 52[b]	70[a], np[b]	90[a], 61[b]
	Thiol (TT)	44[a], 51[b]	49[a], 56[b]	47[a], 42[b]	40[a], 23[b]	31[a], np[b]	43[a], 27[b]
PmA/MDEA/TMPTA	Acrylate	43[a], 10[b]	46[a], 25[b]	30[a], 22[b]	35[a], 8[b]	28[a], np[b]	27[a], np[b]
PmA/Iod/EPOX	Epoxy	np[b]	np[b]	np[b]	np[b]	np[b]	np[b]
PmA/Iod/EPOX/TMPTA	Acrylate	66[a], np[b]	68[a], np[b]	26[a], np[b]	np[a], np[b]	np[a], np[b]	62[a], np[b]
	Epoxy	42[a], np[b]	42[a], np[b]	26[a], np[b]	np[a], np[b]	np[a], np[b]	40[a], np[b]
PmA/Iod/HEA	Acrylate	70[a], 42[b]	74[a], 60[b]	62[a], 40[b]	60[a], 23[b]	12[a], np[b]	64[a], 29[b]
PmA/Iod/HEA/EPOX	Acrylate	79[a], 62[b]	82[a], 61[b]	75[a], 52[b]	66[a], 40[b]	44[a], np[b]	76[a], 48[b]
PA/Iod/TMPTA	Acrylate	66[a], np[b]	57[a], 25[b]	37[a], np[b]	43[a], np[b]	82[a], np[b]	46[a], np[b]
PA/TT/TMPTA	Acrylate	92[a], 90[b]	92[a], 96[b]	86[a], 85[b]	84[a], 46[b]	76[a], np[b]	70[a], np[b]
	Thiol (TT)	40[a], 44[b]	40[a], 50[b]	38[a], 44[b]	31[a], 18[b]	30[a], np[b]	28[a], np[b]
PA/Iod/TT/TMPTA	Acrylate	98[a], 98[b]	100[a], 100[b]	99[a], 99[b]	92[a], 91[b]	71[a], 32[b]	96[a], 96[b]
	Thiol (TT)	51[a], 56[b]	45[a], 56[b]	47[a], 53[b]	45[a], 43[b]	31[a], 25[b]	48[a], 50[b]
PA/MDEA/TMPTA	Acrylate	46[a], 48[b]	53[a], 57[b]	50[a], 46[b]	50[a], 43[b]	45[a], np[b]	53[a], 43[b]
PA/Iod/EPOX	Epoxy	66[b]	62[b]	38[b]	37[b]	np[b]	62[b]
PA/Iod/EPOX/TMPTA	Acrylate	43[a], 44[b]	79[a], 61[b]	70[a], 36[b]	73[a], 39[b]	39[a], np[b]	73[a], 15[b]
	Epoxy	49[a], 57[b]	62[a], 65[b]	53[a], 42[b]	66[a], 41[b]	26[a], np[b]	56[a], 52[b]
PA/Iod/HEA	Acrylate	75[a], 61[b]	82[a], 75[b]	75[a], 62[b]	72[a], 60[b]	55[a], np[b]	71[a], 60[b]

PA/Iod/HEA/EPOX	Acrylate	99[a], 83[b]	100[a], 93[b]	87[a], 76[b]	84[a], 72[b]	50[a], np[b]	99[a], 83[b]

[a]experiments in laminate; [b]experiments under air; conversions determined by RT-FTIR; np = no polymerization.

Application for 3D-printing. Among several 3D-printing techniques, the use of the photochemistry is extremely attractive as new 3D-objects can be synthesized *via* visible-light irradiation in a reduced time from the synergistic combination of photoreactive monomers and suitable photoinitiators[35]. Specifically, novel visible-light photoinitiators absorb the emission light from a 3D-printer, thus generating the photopolymerization reactions of specific monomers layer-by-layer to produce new designed 3D-objects. In this context, we proposed the synthesis of 3D-objects (see Figure 6) under air upon LED@405 nm irradiation with the use of the most efficient photoinitiator described in this study, *i.e* **PA**. Two types of 3D-objects were produced in a short time (< 10 min): 1) an open square cube with 1 cm length and 0.6 cm high and 2) a 3D bar with 3 cm length, 0.5 cm width and 0.2 cm thickness. **PA** appears as an interesting visible-light photosensitizer for 3D-printing applications. This opens the way to the synthesis of novel materials by 3D-printing photopolymerization.

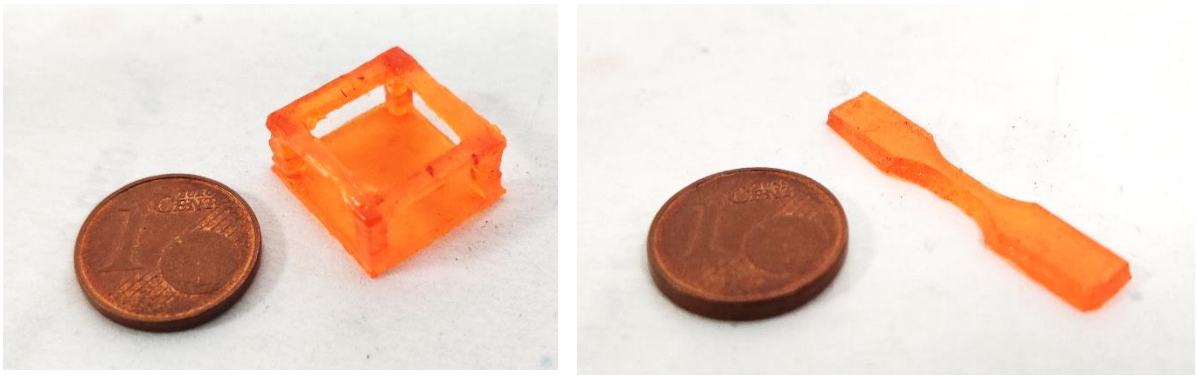

Figure 6. Synthesis of 3D-objects by photopolymerization reaction

Dual role of the photosensitizer: Antibacterial tests. Photodynamic therapy is well-known for cancer treatment and has been recently extended to photodynamic inactivation of bacteria[36-39]. This method allows producing reactive oxygen species (ROS) responsible for bacterial damage. As a result, some materials have demonstrated efficient antibacterial properties against

Gram-positive bacteria when exposed to solar light exposure. However, the synthetic strategies of the current antibacterial systems and their design suffer from information concerning recycling. As demonstrated by Figure S47, **PA** was used as photosensitizer for the synthesis of a new photoactive and recycling antibacterial material against *S. aureus*. Three antimicrobial cycle experiments on the same biomaterial were done for the first time to evaluate its long-term efficiency as biocide agents. Adhesion and proliferation of *S. aureus* have been observed at the surface of the materials even after the third antibacterial cycle experiment (Figure 7). However, when samples are exposed to solar light irradiation, a tremendous inhibition (> 99%) of bacterial adhesion at the surface of the incubated materials is observed whatever the number of the cycles. This could be easily explained by the capability of **PA** to produce singlet oxygen under light irradiation as demonstrated in Figure S48. This result is of great importance as it undoubtedly demonstrates that our material could be re-used without losing its antibacterial properties. Interestingly, no diffusion of the **PA** photoinitiator out of the materials was observed certainly due to its covalent connection to the photoinduced polymer network with the allyl groups.

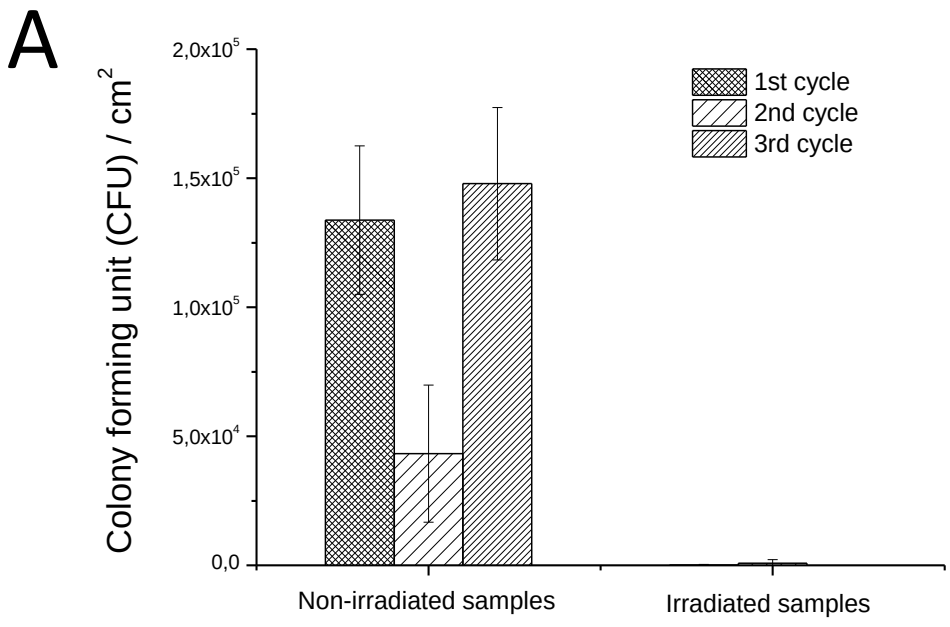

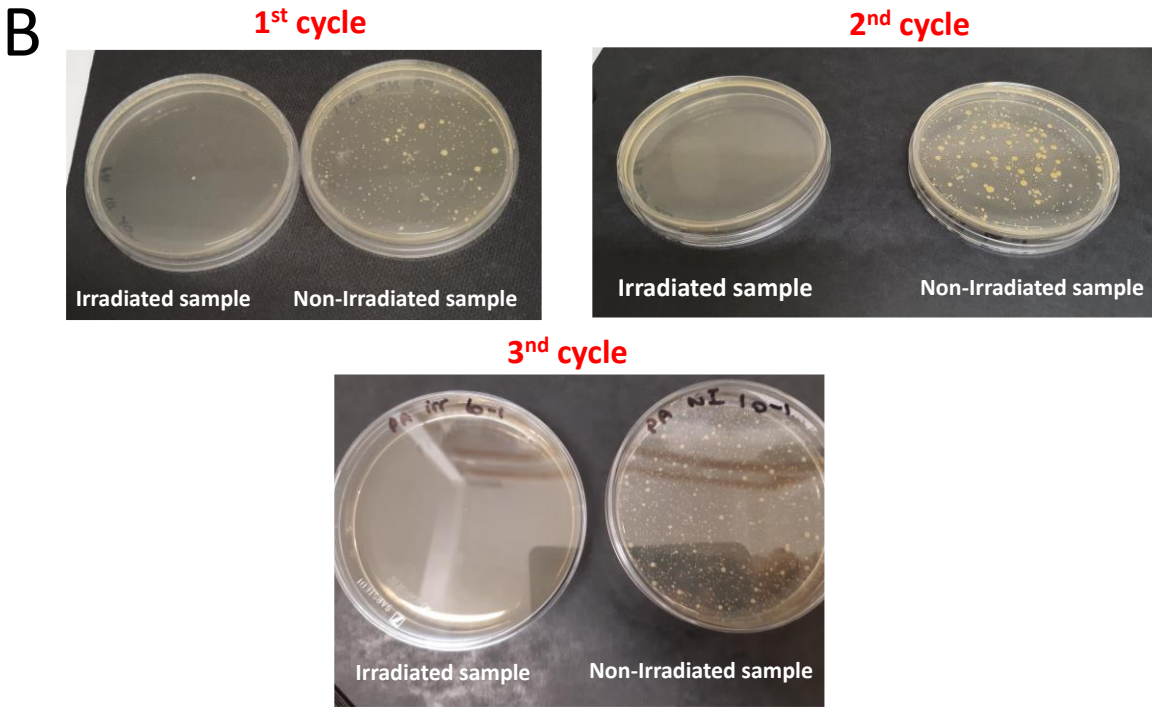

Figure 7. A) Evolution of the Colony Forming Unit (CFUs) at the surface of the material after three antibacterial cycle experiments with and without light exposure and B) optical images of the pietri dishes of the irradiated and non irradiated samples for each of the three antibacterial cycle experiments. The small yellow dots in the petri dishes of the non-irradiated samples correspond to *S. aureus* colonies.

CONCLUSIONS

Purpurin derivatives *i.e.* mono-allylated purpurin (**PmA**) and tri-allylated purpurin (**PA**) in combination with co-initiators (Iod, MDEA or TT) demonstrated performing initiating properties for both FRP and CP under visible-light exposure (LEDs@405 nm, 455 nm, 470 nm, 530 nm and Xe lamp) under air and in oxygen-free conditions. Interestingly, final epoxy and acrylate conversions obtained in laminate or under air with **PA** derived type II photoinitiating systems are more efficient than well-described and common photoinitiating systems described in literature. We also demonstrated that **PA** could be used to design 3D-objects by the 3D-photoprinting technique, in a reduced time. Interestingly, the resulting materials incorporating

PA have undoubtedly demonstrated excellent antibacterial properties with a tremendous inhibition (> 99%) of bacterial adhesion under visible-light exposure, even after three antibacterial cycle experiments, highlighting thus the capability to the material to be recycled.

AUTHOR INFORMATION

Corresponding Author

* Dr. Davy-Louis Versace. versace@icmpe.cnrs.fr

Author Contributions

The manuscript was written through contributions of all authors. All authors have given approval to the final version of the manuscript.

ACKNOWLEDGMENT

Dr Versace Davy-Louis and Prof. Vlasta Brezová would like to thank French National Research Agency (ANR), UPEC, Ministry of Education, Science, Research and Sport of the Slovak Republic for funding within the scheme "Excellent research teams" and Scientific Grant Agency of the Slovak Republic (VEGA Project 1/0064/21) for financial support.

ASSOCIATED CONTENT

Supporting Information.

1D and 2D NMR spectra of **P**, **PmA** and **PA**; additional EPR experiments on **P** or **PmA**/co-initiators; additional steady-state photolysis experiments; determination of quenching rate constants K_{SV} by fluorescence; determination of quenching rate constants k_q by laser flash photolysis; cyclic voltammograms of **P**, **PmA** and **PA**; transition absorption spectra of **P**, **PmA** and **PA**; Decay traces of purpurin derivatives/co-initiators by LFP; photopolymerization

kinetics under air and in laminate; evaluation of the generated singlet oxygen from the visible-light irradiation of **PA**. The following files are available free of charge.

REFERENCES

1. Y. Yagci, S. Jockusch and N. J. Turro, *Macromolecules*, 2010, **43**, 6245-6260.
2. R. S. Davidson, *Exploring the Science, Technology and Applications of UV and EB Curing.*, SITA Technology Ltd, London, 1999.
3. J. P. Fouassier, X. Allonas and D. Burget, *Progr. Org. Coat.* , 2003, **47**, 16-36.
4. P. Xiao, J. Zhang, F. Dumur, M. A. Tehfe, F. Morlet-Savary, B. Graff, D. Gigmes, J.-P. Fouassier and J. Lalevée, *Prog. Polym. Sci.*, 2015, **41**, 32-66.
5. S. C. Ligon, B. Husár, H. Wutzel, R. Holman and R. Liska, *Chem. Rev.* , 2014, **114**, 557-589.
6. J. P. Fouassier and J. Lalevée, *Photoinitiators for Polymer Synthesis: Scope, Reactivity, and Efficiency*, John Wiley & Sons, Inc., 2013.
7. B. Steyrer, P. Neubauer, R. Liska and J. Stampfl, *Materials*, 2017, **10**, 1445.
8. J. P. Fouassier and J. Lalevée, *Photopolymerisation Initiating Systems* Royal Society of Chemical 2018.
9. H. L. Needles, *J. Polym. Sci. Part B: Polym. Lett.*, 1967, **5**, 595-600.
10. H. L. Needles and W. L. Wasley, *Text. Res. J.*, 1969, **39**, 97-98.
11. A. Mishra and S. Daswal, *Colloid Polym. Sci.*, 2007, **285**, 1109-1117.
12. J. V. Crivello and U. Bulut, *J. Polym. Sci. Part A: Polym. Chem.*, 2005, **43**, 5217-5231.
13. M. Condat, P. E. Mazeran, J. P. Malval, J. Lalevée, F. Morlet-Savary, E. Renard, V. Langlois, S. Abbad Andalloussi and D. L. Versace, *RSC Adv.*, 2015, **5**, 85214-85224.
14. M. Condat, J. Babinot, S. Tomane, J.-P. Malval, I.-K. Kang, F. Spillebout, P.-E. Mazeran, J. Lalevée, S. A. Andalloussi and D.-L. Versace, *RSC Adv.*, 2016, **6**, 18235-18245.
15. P. Sautrot-Ba, J.-P. Malval, M. Weiss-Maurin, J. Paul, A. Blacha-Grzechnik, S. Tomane, P.-E. Mazeran, J. Lalevée, V. Langlois and D.-L. Versace, *ACS Sustain. Chem. Eng.*, 2018, **6**, 104-109.
16. H. Bhajan Singh and K. Avinash Bharati, *Handbook of Natural Dyes and Pigments*, Woodhead Publishing India, 2015.
17. F. Alihosseini and G. Sun, in *Functional Textiles for Improved Performance, Protection and Health*, eds. N. Pan and G. Sun, Woodhead Publishing, 2011, DOI: https://doi.org/10.1533/9780857092878.376, pp. 376-403.
18. S. Har Bhajan and K. A. Bharati, in *Handbook of Natural Dyes and Pigments*, eds. S. Har Bhajan and K. A. Bharati, Woodhead Publishing India, 2014, DOI: https://doi.org/10.1016/B978-93-80308-54-8.50006-X, pp. 33-260.
19. P. Sautrot-Ba, S. Jockusch, J.-P. Malval, V. Brezová, M. Rivard, S. Abbad-Andaloussi, A. Blacha-Grzechnik and D.-L. Versace, *Macromolecules*, 2020, **53**, 1129-1141.
20. L. Breloy, R. Losantos, D. Sampedro, M. Marazzi, J.-P. Malval, Y. Heo, J. Akimoto, Y. Ito, V. Brezová and D.-L. Versace, *Polym. Chem.*, 2020, **11**, 4297-4312.
21. S. Stoll and A. Schweiger, *J. Magn. Reson.* , 2006, **178**, 42-55.
22. M. Neda, K. Okinaga and M. Shibata, *Mater. Chem. Phys.*, 2014, **148**, 319-327.
23. G. R. Buettner, *Free Rad. Biol. Med.*, 1987, **3**, 259-303.
24. E. G. Janzen, *Can. J. Chem.* , 1984, **62**, 1653–1657.
25. D. Rehm and A. Weller, *Isr. J. Chem.* , 1970, **8**, 259-271.

26. S. Peter Pappas, B. C. Pappas, L. R. Gatechair and W. Schnabel, *J. Polym. Sci.: Polym. Chem. Ed.* , 1984, **22**, 69-76.
27. J. Zhang, J. Lalevée, J. Zhao, B. Graff, M. H. Stenzel and P. Xiao, *Polym. Chem.*, 2016, **7**, 7316-7324.
28. H. Görner, *Photochem. Photobiol.*, 2003, **77**, 171-179.
29. Z. Machatová, Z. Barbieriková, P. Poliak, V. Jančovičová, V. Lukeš and V. Brezová, *Dyes Pigm.*, 2016, **132**, 79-93.
30. J. A. Pedersen and R. H. Thomson, *J. Magn. Reson. (1969)*, 1981, **43**, 373-386.
31. S. Rahimipour, I. Bilkis, V. Péron, G. Gescheidt, F. Barbosa, Y. Mazur, Y. Koch, L. Weiner and M. Fridkin, *Photochem. Photobiol.*, 2001, **74**, 226-236.
32. A. V. Bulatov, G. P. Voskerchyan, S. N. Dobryakov and A. T. Nikitaev, *Russ. Chem. Bull.*, 1986, **35**, 747-751.
33. L. Breloy, V. Brezová, A. Blacha-Grzechnik, M. Presset, M. S. Yildirim, I. Yilmaz, Y. Yagci and D.-L. Versace, *Macromolecules*, 2020, **53**, 112-124.
34. J. L. Kice, *J. Polym. Sci.* , 1956, **19**, 123-140.
35. A. Bagheri and J. Jin, *ACS Appl. Polym. Mater.*, 2019, **1**, 593-611.
36. L. Huang, T. Dai and M. R. Hamblin, *Methods Mol Biol*, 2010, **635**, 155-173.
37. M. Tim, *J. Photochem. Photobiol. B: Biol.*, 2015, **150**, 2-10.
38. C. S. Vinagreiro, A. Zangirolami, F. A. Schaberle, S. C. C. Nunes, K. C. Blanco, N. M. Inada, G. J. da Silva, A. A. C. C. Pais, V. S. Bagnato, L. G. Arnaut and M. M. Pereira, *ACS Infect. Dis.*, 2020, **6**, 1517-1526.
39. A. Wozniak and M. Grinholc, *Front. Microbiol.*, 2018, **9**.